Published in final edited form as:
Neuroimage. 2012 April 2; 60(2): 1266–1279. doi:10.1016/j.neuroimage.2012.01.098.

Measuring longitudinal change in the hippocampal formation from in vivo high-resolution T2-weighted MRI

Sandhitsu R. Das[a,*], **Brian B. Avants**[a], **John Pluta**[a], **Hongzhi Wang**[a], **Jung W. Suh**[a], **Michael W. Weiner**[b], **Susanne G. Mueller**[b], and **Paul A. Yushkevich**[a]

[a]Penn Image Computing and Science Laboratory (PICSL), Department of Radiology, University of Pennsylvania, Philadelphia, PA, USA

[b]Department of Veterans Affairs Medical Center, University of California at San Francisco and Center for Imaging of Neurodegenerative Diseases, San Francisco, CA, USA

Abstract

The hippocampal formation (HF) is a brain structure of great interest because of its central role in learning and memory, and its associated vulnerability to several neurological disorders. In vivo oblique coronal T2-weighted MRI with high in-plane resolution (~0.5 mm×0.5 mm), thick slices (~2.0 mm), and a field of view tailored to imaging the hippocampal formation (denoted HF-MRI in this paper) has been advanced as a useful imaging modality for detailed hippocampal morphometry. Cross-sectional analysis of volume measurements derived from HF-MRI has shown the modality's promise to yield sensitive imaging-based biomarker for neurological disorders such as Alzheimer's disease. However, the utility of this modality for making measurements of longitudinal change has not yet been demonstrated. In this paper, using an unbiased deformation-based morphometry (DBM) pipeline, we examine the suitability of HF-MRI for estimating longitudinal change by comparing atrophy rates measured in the whole hippocampus from this modality with those measured from more common isotropic (~1 mm^3) T1-weighted MRI in the same set of individuals, in a cohort of healthy controls and patients with cognitive impairment. While measurements obtained from HF-MRI were largely consistent with those obtained from T1-MRI, HF-MRI yielded slightly larger group effect of greater atrophy rates in patients than in controls. The estimated minimum sample size required for detecting a 25% change in patients' atrophy rate in the hippocampus compared to the control group with a statistical power β=0.8 was N=269. For T1-MRI, the equivalent sample size was N=325. Using a dataset of test–retest scans, we show that the measurements were free of additive bias. We also demonstrate that these results were not a confound of certain methodological choices made in the DBM pipeline to address the challenges of making longitudinal measurements from HF-MRI, using a region of interest (ROI) around the HF to globally align serial images, followed by slice-by-slice deformable registration to measure local volume change. Additionally, we present a preliminary study of atrophy rate measurements within hippocampal subfields using HF-MRI. Cross-sectional differences in atrophy rates were detected in several subfields.

Keywords

Hippocampus; Subfields; T1-weighted; T2-weighted; MRI; Longitudinal; Atrophy; MCI; Evaluation; Medial temporal lobe; Deformation-based morphometry; DBM sample size

* Corresponding author. sudas@seas.upenn.edu. .

Introduction

The hippocampal formation (HF) is widely studied by clinicians and neuroscientists alike, owing to its central role in cognitive processing, particularly in processes mediating learning and memory (Squire et al., 2004). Structural as well as functional measurements in the hippocampal region of interest (ROI) and its neighboring medial temporal lobe (MTL) structures have been successfully used as imaging-based biomarkers of brain pathology in several neurological disorders. Hippocampal volume, measured using structural MRI, is significantly reduced in Alzheimer's Disease (AD) (Jack et al., 1992) and in its prodromal stages (de Leon et al., 1997), in other neurodegenerative disorders such as semantic dementia (Chan et al., 2001), as well as in psychiatric disorders such as schizophrenia (Bogerts et al., 1993), and other neurological conditions (a review can be found in (Geuze et al., 2005)).

While such cross-sectional volumetry studies provide useful clinical information, a great deal of emphasis has been placed in the recent literature on MRI-based measurements of longitudinal change in the hippocampal volume. It has been hypothesized that the estimates of hippocampal atrophy rate derived from such measures will play a key role in reducing the cost and duration of clinical trials for disease-modifying pharmaceutical treatments in AD and other neurodegenerative diseases (Jack et al., 2010). Among the various biomarkers proposed for such clinical trials, MRI-based hippocampal atrophy estimates are thought to offer the best combination of sensitivity to disease progression in the early symptomatic stages of the disease and robustness to repeat measurement errors (Caroli et al., 2010).

Longitudinal change in the hippocampus measured from MRI has been studied for more than a decade (Du et al., 2004; Fox et al., 1996; Fox et al., 2005; Fuerst et al., 2003; Hashimoto et al., 2005; Jack et al., 1998; Jack et al., 2003; Kaye et al., 2005; Leung et al., 2010; Ridha et al., 2006; Rohrer et al., 2008; Schuff et al., 2009; Steffens et al., 2011; Thompson et al., 2004; Wang et al., 2003). Atrophy rates in the hippocampus have been measured in clinical populations such as Alzheimer's disease (AD) (Fox et al., 1996; Jack et al., 1998; Ridha et al., 2006), depression (Steffens et al., 2011), epilepsy Fuerst et al., 2003 and non-AD dementia (Rohrer et al., 2008). Typically, such studies use one of a few well-established longitudinal measurement techniques, such as deformation-based morphometry (DBM) (Chung et al., 2001; Leow et al., 2006; Studholme et al., 2004), brainboundary shift integral (BSI) (Barnes et al., 2004; Freeborough and Fox, 1997; Leung et al., 2010), anatomical surface-based shape modeling (Csernansky et al., 2000; Thompson et al., 1996; Thompson et al., 2004; Wang et al., 2003) or manual labeling of serial images (Fox et al., 2005; Jack et al., 2003; Kaye et al., 2005). In particular, large studies using the Alzheimer's Disease Neuroimaging Initiative (ADNI) dataset (Schuff et al., 2009; Schott et al., 2010; Wolz et al., 2010; Yushkevich et al., 2010a) that employed some of these techniques have characterized the hippocampal longitudinal atrophy patterns in the AD and mild cognitive impairment (MCI) extensively. A more complete review of hippocampal atrophy rate measurements reported in the literature can be found in Barnes et al. (2009). Group effects between elderly controls and individuals with MCI, which is frequently a preclinical stage of AD, have been found (Jack et al., 2000; Apostolova et al., 2010; Leung et al., 2010; Schott et al., 2010; Wolz et al., 2010). Many recent studies have provided estimates of sample sizes required to detect a given amount of change in the HF and other MTL regions during a clinical trial (Holland et al., 2011). This extensive body of work underscores the importance of longitudinal change measurements in the HF.

Prior studies of longitudinal change in the HF have typically used the same approaches as whole-brain longitudinal studies, and thus relied almost exclusively on T1-weighted MRI (T1-MRI), usually with nearly isotropic ~1 mm^3 resolution. By contrast, in cross-sectional

studies of the HF, much attention has recently been placed on alternative MRI protocols that are more tailored for imaging the HF and other medial temporal lobe (MTL) structures (Kerchner et al., 2010; La Joie et al., 2010; Mueller et al., 2008; Malykhin et al., 2010; Prudent et al., 2010; Small et al., 2000; Thomas et al., 2008; Theysohn et al., 2009; Van Leemput et al., 2009; Zeineh et al., 2003). In particular, superior intensity contrast in the HF can be obtained using T2-weighted MRI (Fig. 1) with high in-plane spatial resolution, oblique slice orientation perpendicular to the long axis of the hippocampus (Fig. 1), and high slice thickness. We use the term HF-MRI to describe this type of MRI scan, both for brevity, and to emphasize that unlike most clinical T2-weighted MRI scans, the field of view, resolution, and orientation are chosen with the specific goal of imaging the HF and nearby MTL structures. A particular appeal of HF-MRI is the improved visibility of anatomical landmarks in the hippocampal region, specifically, of a hypointense band thought represent myelinated fibers in the stratummoleculare/lacunosum (Eriksson et al., 2008). This property has led researchers to label the subfields of the HF in HF-MRI, and estimate their volume (Mueller et al., 2007; Malykhin et al., 2010). It has been hypothesized that such subfield-specific hippocampal volume measures will prove more sensitive to disease effects than whole hippocampus volume measures. This hypothesis stems from the selective vulnerability of these subregions to pathological processes (Huesgen et al., 1993; Sass et al., 1991; Saravia et al., 2006). Indeed, cross-sectional studies that used HF-MRI have found patterns of disease-related atrophy in the HF in various neurological disorders (Mueller et al., 2009; Mueller et al., 2010), largely consistent with pathological findings in these diseases.

Despite the proven suitability of HF-MRI for cross-sectional imaging and morphometry of the HF, this modality has not yet been leveraged for making longitudinal change measurements. If it could be shown that HF-MRI shares the robustness and sensitivity to longitudinal change that T1-MRI offers, this would potentially open the door for making robust and sensitive subfield-specific atrophy rate measurements in the HF. This would be particularly relevant for AD research, where subfields are known to differ in the stage of the disease where they first become affected (Braak and Braak, 1991; Bobinski et al., 1997; Jacobsen et al., 2006) and in the subsequent rate of neurodegeneration.

However, different modalities of MRI inherently vary in the amount of tissue contrast, the noise profile, and other acquisition parameters — all of which can affect the measurements of change in a structure of interest. In the case of HF-MRI, a particular confounding factor is the highly anisotropic nature of the images, compared to the isotropic T1-weighted MRI. This can negatively impact the quality of spatial normalization between serial images, a key step in the commonly used deformation-based morphometry (DBM) approach for measuring longitudinal change. Therefore, as a first step towards realizing the full potential of HF-MRI for making subfield-specific longitudinal measurements, there is a need to validate measures of change made from this imaging modality.

Therefore, the primary goal of this paper is to perform an evaluation of the suitability of HF-MRI for longitudinal analysis. To this end, we evaluate its ability to detect differences in hippocampal atrophy rates between healthy elderly controls and patients with cognitive impairment, as well as evaluate the robustness of HF-MRI measurements in test-retest data. Analyzing data from a cohort where subjects had both longitudinal T1-MRI and HF-MRI scans available, we find that HF-MRI measurements are highly consistent with those from T1-MRI; detect slightly greater group effects in atrophy rates between patients and controls; and are slightly more robust to repeat measurement error than T1-MRI.

We use slight modifications of the conventional DBM framework used in T1-MRI to process HF-MRI data, to address the image normalization challenges posed by anisotropic

spatial resolution of the latter. In order to demonstrate that the improved sensitivity of HF-MRI is driven by the inherent properties of the modality, rather than being an artifact of these methodological choices, we repeat longitudinal analysis in both modalities using several variants of the DBM framework. We find that indeed, the improved sensitivity of HF-MRI does not arise from methodological confounds.

Finally, since the eventual goal of using HF-MRI in longitudinal studies is to obtain subfield-specific measurements, we present a preliminary study examining atrophy rates in HF subfield ROIs in our clinical dataset. We observe non-uniform atrophy rates across subfields.

Materials and methods

Subjects

Clinical cohort—The subjects in this cohort had been recruited for an NIH-sponsored study on prediction of cognitive decline using MRI (R01 AG010897, PI: author MW). Eligible subjects were over 60 yrs of age who reported subjective memory problems but were not demented. All subjects underwent a medical examination and standardized laboratory and neuropsychological assessment. Subjects suffering from medical conditions or taking medications affecting cognitive performance were excluded as were subjects with a history of brain trauma, brain surgery or evidence for stroke (exception: white matter hyperintensities or small lacunes), and skull defects on the MRI. The subjects included in this study were selected from a larger population recruited for this project because they had a baseline MR exam and at least one follow up MR exam of suitable quality at the time of the preparation of this manuscript. Eight subjects had been diagnosed with amnestic mild cognitive impairment (aMCI) according to the criteria of Petersen et al. (1999) (age 70±8 yrs), another 7 were cognitively impaired (executive or memory deficits), but did not meet the formal criteria for aMCI (age 76±9 yrs); these 15 subjects (age 72±8 yrs) were grouped together as patients. In addition, there were 25 age-matched cognitively intact elderly controls (age 69±7 yrs). Followup scans were acquired between one and three years after the baseline scan.

Test–retest cohort—In a separate test–retest cohort of 9 healthy controls (age 42±16 yrs), subjects were scanned in two separate sessions on the same day with at least 2 h between scans, and slightly different head positions in the scanner. The same scanning protocol as in the clinical cohort was used in both sessions.

Image acquisition

Imaging was performed on a Bruker MedSpec 4 T system controlled by a Siemens Trio™ console using a USA instruments eight channel array coil that consisted of a separate transmit coil enclosing the eight receiver coils. The following sequences, which were part of a larger research imaging and spectroscopy protocol, were acquired: 1. 3D T1-weighted gradient echo MRI (MPRAGE) TR/TE/TI=2300/3/950 ms, 7° flip angle, 1.0×1.0×1.0 mm^3 resolution, FOV 256×256×176, acquisition time 5.17 min (referred to as T1-MRI), 2. high resolution T2 weighted turbo spin echo sequence (TR/TE: 3990/21 ms, a relatively short TE chosen for improved signal-to-noise ratio), with 15 spin echoes per excitation for k-space encoding, 18.6 ms echo spacing and low SAR refocusing pulses of a 149° flip angle, 100% oversampling in the phase encoding direction to reduce aliasing, 0.4×0.5 mm nominal in-plane resolution, 2 mm slice thickness, 24 interleaved slices without gap, acquisition time 3:23 min (adapted from (De Vita et al., 2003; Thomas et al., 2004)), angulated perpendicular to the long axis of the hippocampal formation (referred to as HF-MRI). This sequence

covers the anterior two-thirds of the hippocampal formation in all subjects but misses parts of the tail in most subjects. Examples of T1- and T2-weighted images are shown in Fig. 1.

Segmentation of baseline images

Segmentation of baseline HF-MRI was performed using the automatic labeling technique described in (Yushkevich et al., 2010b). The method combines multi-atlas segmentation, similarity-weighted voting, and a learning-based bias correction technique to label the HF subregions. In the *hippocampus proper*, HEAD, BODY and TAIL labels provide a coarse level of subdivision. In the BODY region, the interior structure of the hippocampus follows a consistent pattern, with the main hippocampal layers clearly separated by the *dark band* composed of stratum radiatum and stratum lucidum of the CA. Thus, the BODY region was divided into CA1, CA2, CA3 and CA4/dentate gyrus (CA4DG) subfields. The CA4DG label consists of the thin strip of tissue called stratum moleculare of DG, and the dentate hilus, sometimes referred to as CA4 (Amaral and Lavenex, 2007; Duvernoy, 2005). Three ROIs outside of the hippocampus proper (extra-hippocampal regions) were also labeled: subiculum (SUB), entorhinal cortex (ERC) and parahippocampal gyrus (PHG). Part of the subiculum was included in the HEAD label, as well as in the CA1 label in the BODY region. The accuracy of labeling, as reported in (Yushkevich et al., 2010b), is comparable to the overlap between manual segmentations by trained raters. A detailed description of the segmentation protocol can be found in the *Supplementary Information* of (Yushkevich et al., 2010b). Labeling accuracy of smaller subfields CA2 and CA3 are much lower than those of the larger ones such as CA4DG and CA1. Therefore, we chose not to separately analyze measurements within these ROIs. Instead, we included CA2, CA3 and CA4DG into a combined CA234DG label, similar to what previous studies have done (Zeineh et al., 2003). The combination of CA and DG subfields, and HEAD and TAIL labels make up the whole hippocampus label in HF-MRI.

A similar multi-atlas segmentation technique was used to segment the whole hippocampus in T1-MRI (Wang et al., 2011). Accuracy of this labeling is highly competitive with the state-of-the-art automatic hippocampus segmentation methods. The protocol used to define the whole hippocampus differs from that used in HF-MRI. T1-MRI includes a greater extent of the posterior aspect of the hippocampus. Also, the extent of the subiculum included in the whole hippocampus ROI is lesser in the T1-MRI protocol than in HF-MRI. The details of the T1-MRI segmentation protocol can be found in Pluta et al. (2009).

Processing pipeline for longitudinal change measurements from HF-MRI

The deformation-based morphometry (DBM) pipeline for making longitudinal change measurements within an ROI consists of the steps outlined below. Fig. 2 provides an overview of the processing pipeline.

Linear registration—Rigid registration is used to bring baseline and followup MRI of each subject into global alignment. The FLIRT tool from the FSL software suite (Smith et al., 2004) is used for all linear registrations. The normalized cross-correlation metric is used for intra-modality registrations and normalized mutual information is used for inter-modality registration, all with a 6-parameter rigid registration framework.

Initialization—Since HF-MRI only images a few slices covering the HF, the bounding boxes of the baseline and followup images may not contain exactly the same anatomical volume, making direct alignment difficult. To address this, we use the whole brain T1-MRI images to obtain an initial alignment between the time points. We denote this transformation matrix as M_{T1}^{WB}, where WB stands for whole brain. The HF-MRI image is then rigidly aligned with the T1-MRI at the corresponding time point, which corrects for head motion

between scans. We denote these inter-modality transformations for baseline (BL) and followup (FU) time points by M^{BL}_{T1-T2} and M^{FU}_{T1-T2} respectively. Combining the inter-modality transformations with the intra-modality one gives the initial alignment M^{init}_{T2} of baseline and followup HF-MRI:

$$M^{init}_{T2} = M^{FU}_{T1-T2} \times M^{WB}_{T1} \times M^{BL^{-1}}_{T1-T2}. \quad (1)$$

ROI-based linear registration of longitudinal HF-MRI: As our goal is to produce accurate estimates of change in the HF, we note that registering a small ROI around the HF in both images instead of registering the whole brain images will suffice, and may align the HF more precisely. This is because the optimization for rigid alignment of ROI images only considers voxels around the HF. Optimizing over the whole brain, on the other hand, may be optimal for overall alignment of the intracranial cavity, but may be suboptimal for alignment of the HF. An additional factor in case of HF-MRI is that because of thick slices (2.0 mm slice thickness), even a small residual error in the rotation parameter can lead to a relatively large misalignment in certain parts of the image, depending on where the axis of rotation is. We define an ROI around the HF in each hemisphere in the baseline image using the baseline HF segmentation consisting of all voxels within 10 mm of the hippocampal mask in all three dimensions and crop the images around this ROI (see insets in Figs. 1(e)–(h)). A similar ROI is also defined in the followup image by using the hippocampal mask transformed to the followup image using M^{init}_{T2}. The cropped serial image pairs of the HF ROI for left and right hemispheres are then independently aligned. Left and right linear registrations are initialized by the initial transformation M^{init}_{T2}. This produces the final rigid transform matrices for left and right HF ROI, denoted as M^{left}_{T2} and M^{right}_{T2}. We call this ROI-based approach to global registration ROI-RIGID, as opposed to the traditional approach (WB-RIGID) where whole brain images are globally aligned. Fig. 3 shows an example to visually illustrate the difference between WB-RIGID and ROI-RIGID alignment in HF-MRI. Comparing difference images in panels (c) and (d) clearly demonstrates superior alignment of HF-ROI using ROI-RIGID. Although the improvement in alignment may not be as clearly visible for all subjects as in the example of Fig. 3, image similarity metric improves using ROI-RIGID in a majority of the subjects (for this subject, there was an improvement of 1.3% in the similarity metric value).

Deformable registration

Deformable registration—Deformable registration between baseline and followup images is a commonly used technique that provides measurements of longitudinal change (Thompson and Toga, 1998; Chung et al., 2001). A deformable mapping is computed between the baseline and followup images after application of the global transformation. It generates a locally varying point-by-point correspondence map between a pair of images, subject to a measure of image similarity between the corresponding pairs of points being maximized. In this study, the SyN diffeomorphic registration method (Avants et al., 2008), as implemented in the ANTs (http://www.picsl.upenn.edu/ANTS) toolkit was used. Briefly, SyN optimizes an energy function that has a symmetric formulation with respect to input images I and J, with the similarity metric to be minimized given by

$$\pi \left[I\left(\phi_1\left(\mathbf{x}, 1\right)\right), J\left(\phi_2\left(\mathbf{x}, 1\right)\right)\right] \quad (2)$$

where $\phi_1(\mathbf{x},t)$ and $\phi_2(\mathbf{x},t)$ represent time-dependent mappings of the image domain Ω onto itself, $t \in (0, 1)$ is the time parameter, and the operator $\pi[.,.]$ measures the amount of dissimilarity between a pair of images.

Unbiased registration—As has been discussed extensively in the literature (Fox et al., 2011; Hua et al., 2011; Reuter et al., 2010; Smith et al., 2002; Thompson et al., 2011; Yushkevich et al., 2010a), to ensure unbiased longitudinal measurements, it is important to compute the image similarity metric π in a symmetric fashion, so that both images undergo the same number of resampling operations, as well as the same amount of global transformation before applying the deformable transformations ϕ_1 and ϕ_2 and measuring similarity between them. Let $R_{ref}(I, \Psi)$ define a resampling operator that produces an image I', which is resampled in the space of a reference image I_{ref}, from an image I after applying a spatial transformation Ψ. If I and I_{ref} are defined on a lattice of points $\{\mathbf{x}_i\} \in \Omega$ and $\{\mathbf{y}_j\} \in \Omega_{ref}$ respectively, we have

$$I'(\mathbf{y}_j) = \sum_i \mathcal{L}(\psi(\mathbf{y}_j) - \mathbf{x}_i) I(\mathbf{x}_i)$$

where $\mathcal{L}$ is an interpolation kernel. We use a tent function which corresponds to linear interpolation. If M is the derived global transformation matrix between the baseline and followup images I^{BL} and I^{FU} respectively, following (Yushkevich et al., 2010a), symmetric computation of π is given by

$$\pi\left[R_{ref}\left(R_{ref}\left(I^{BL}, M^{-\frac{1}{2}}\right), \phi_1\right), R_{ref}\left(R_{ref}\left(I^{FU}, M^{\frac{1}{2}}\right), \phi_2\right)\right]. \quad (3)$$

The operator R_{ref} used in Yushkevich et al. (2010a) resamples both baseline and followup images in the space of the baseline image. Thus, even though equal amount of global transformation is applied to both images, the metric computation is performed in the baseline image space, another potential source of bias (Reuter et al., 2010), which may be more critical in an anisotropic modality like HF-MRI. To eliminate this bias, we resample both images in the space of an image I_{HW} whose lattice is located halfway between the lattices of the two images. Thus, we use $R_{ref}(\cdot,\cdot) = R_{HW}(\cdot,\cdot)$ for all experiments reported here.

Slice-by-slice 2D registration—Due to the highly anisotropic nature of the HF-MRI data, detecting deformations along the slice direction may be difficult because of thick slices, and less reliable than *in-plane* deformations within each oblique slice along the long axis of the hippocampus. Also, the slice thickness is larger than the expected amount of boundary shift due to atrophy — thus, through-plane deformations are harder to interpret. If rigid registration is accurate enough so that corresponding slices in the globally aligned pair of images can be assumed to represent the same anatomy, one can make measurements of change independently within each slice. Therefore, after resampling the ROI image pairs in each hemisphere following symmetric application of the rigid transformation, as given in Eq. (3), we register the corresponding slices of the two images using 2D deformable registration. We note that no additional interpolation is needed to extract the corresponding slices, as both images in Eq. (3) are resampled in the halfway image space. If there are N slices, we simply perform N 2D registrations, each between the *i-th* slices of the two images. This approach is analogous to slice-by-slice registration often used in tagged cardiac MR image analysis for motion estimation (Kerwin et al., 2000). In addition to possible elimination of registration artifacts arising out of the anisotropic data, 2D registration is faster. Panels (e)–(f) in Fig. 3 shows an example of difference map after 2D deformable mapping.

Implementation details—The normalized cross-correlation image similarity metric with a radius of four voxels in each dimension is used for the deformable registration. We use only one (native) resolution level, as the deformations we wish to detect within small

hippocampal subregions are very local in nature. We use 60 iterations of optimization, as the registration algorithm converged in less than 60 iterations in all cases. The input images themselves are not smoothed before metric computation. The step size in the time dimension is 0.25, the default in ANTs. A Gaussian regularizer is used with the following parameters: gradient field σ=0.8 mm, deformation field σ=0.2 mm. To enhance spatial specificity of measurements, regularization amount is intentionally kept low.

Measuring longitudinal change within an ROI

Atrophy rate measurement—Deformable registration and subsequent atrophy rate estimation are performed in the space of the halfway image I_{HW}. Traditional DBM uses Jacobian determinant of the deformation field to estimate local change. However, its computation requires computing spatial derivatives of ϕ, which is computed in the discrete domain using finite difference approximation. This mixes information from a number of neighboring voxels. Further, to avoid numerical errors, the deformation field needs to be very smooth. Since we are interested in subtle changes over narrow regions, we wanted to limit unnecessary smoothing of the deformation field, and cross-contamination from adjacent ROIs. This motivated us to consider an alternative, more direct, way of measuring atrophy using a simple mesh-based approach as we did in our previous work (Yushkevich et al., 2010a). For each slice, the baseline ROI label is fitted with a 2D mesh with triangular elements. The 2D deformation field is applied to mesh vertices. The sum of the areas of triangular elements over meshes in all slices multiplied by the slice thickness, computed before and after application of the deformation field, provides estimates of baseline volume V_{bl} and followup volume V_{fu} respectively. The Triangle (Shewchuk, 1996) software package is used for 2D mesh generation. Let t be the time interval in years between the baseline and followup scans. We then compute annualized atrophy rate as

$$A = \frac{\left(V_{bl} - V_{fu}\right)}{V_{bl} \times t}. \quad (4)$$

Processing pipeline for longitudinal change measurements from T1-MRI

Longitudinal measurements in T1-MRI are obtained as a comparison with those obtained using HF-MRI in the same subjects. For T1-MRI, the DBM pipeline commonly used in the literature is used, as described below.

Linear registration—Rigid registration of serial T1-MRI uses the conventional WB-RIGID approach, where whole brain images are globally aligned, producing the global transformation matrix M_{T1}^{WB}.

Deformable registration—The same unbiased longitudinal processing is used in T1-MRI as described for HF-MRI in the Deformable registration section describing processing for HF-MRI, except that ROI image pairs around the HF are mapped using 3D registration. Registration parameters are same as those for HF-MRI, other than the regularization parameters: gradient field σ=2.0 mm, deformation field σ=0.5 mm. Regularization parameter values are chosen to be proportional to the in-plane resolution of the respective modalities.

Measuring longitudinal change within an ROI—Atrophy rates are measured using a mesh-based approach similar to that used for HF-MRI. We fit a volumetric mesh consisting of tetrahedral elements to each ROI label in the baseline image. The sum of volumes of all the mesh elements is taken as baseline volume V_{bl}. We apply the 3D deformation field to

each vertex of the mesh and recompute and add the volumes after deformation — this gives us an estimate of followup volume V_{fu}. Atrophy is then computed as change per unit volume as in Eq. (4). The TetGen (http://tetgen.berlios.de) software package is used for 3D mesh generation.

Statistical analysis of clinical dataset

After atrophy rates A are computed for all subjects, one-sample t-test is used to assess significant non-zero change within each subject group, and two-sample t-test is used to assess significant group difference in atrophy rates between patients and controls. For each experiment, we also perform power analysis and report effect size Δ, as well as sample size estimate N, and use this to evaluate the clinical utility of the approach. Sample size is estimated as the total number of subjects required in a hypothetical one-year clinical trial to detect a 25% reduction in patient atrophy rate compared to the control atrophy rate. The sample size calculation is performed with a desired statistical power β=0.8 at a level of significance α=0.05 for a one-sided alternative hypothesis with a null hypothesis of no group effect. Effect size Δ and sample size N are computed as

$$\Delta = \frac{\bar{A}_{PAT} - \bar{A}_{CTL}}{s_{PAT}}, \quad (5)$$

$$N = 2\left(\frac{\left(z_{1-\alpha} + z_{\beta}\right) s_{PAT}}{0.25\left(\bar{A}_{PAT} - \bar{A}_{CTL}\right)} \right)^2, \quad (6)$$

where z_t is the t-th quantile of the standard normal variate, $\bar{A}_{PAT}$ and $\bar{A}_{CTL}$ are mean atrophy rates in patients and controls respectively, and s_{PAT} is the standard deviation of patient atrophy rates. In contrast to a number of studies (Beckett et al., 2010; Jack et al., 2010; Risacher et al., 2010) that derived sample sizes based on a criterion for detecting an absolute change in patient atrophy rate, we base sample size estimates on relative change in patient atrophy rate, as recommended by various authors (Fox et al., 2000; Holland et al., 2011; Yushkevich et al., 2010a), as a way to avoid possible underestimation of sample size due to methodological bias and due to failure to account for age-related changes in the hippocampus.

Statistical analysis of test-retest dataset

“Pseudo atrophy rates” are computed as measured change between the pair of scans in each subject in the test–retest dataset, treating one of the scans randomly as followup, and using methods described in the Processing pipeline for longitudinal change measurements from HF-MRI section and the Processing pipeline for longitudinal change measurements from T1-MRI section for HF-MRI and T1-MRI, respectively. One sample t-test is used to assess whether any significant *change* is detected, which would indicate an additive bias in the measurements.

One possible source of variance in longitudinal measurements from HF-MRI is the slightly different slice prescriptions during the followup scan compared to the baseline scan. The operator manually prescribes the orientation of the oblique coronal slices such that it’s perpendicular to the long axis of the hippocampus, based on sagittal view of T1-MRI. However, some difference in the orientation still remains. We computed this difference in orientation between oblique coronal slices as an angle projected onto the sagittal plane for each repeat scan pair and correlated this against the measured atrophy rate.

Confounds due to methodological choice and anatomical definition of hippocampus

As described in the Processing pipeline for longitudinal change measurements from HF-MRI section and the Processing pipeline for longitudinal change measurements from T1-MRI section, the HF-MRI longitudinal DBM pipeline uses slightly different methodological components than the T1-MRI pipeline (i.e. ROI-RIGID vs. WB-RIGID linear registration; 2D vs. 3D deformable registration) primarily due to the anisotropic nature of the data. Thus, when comparing atrophy rates computed using DBM in T1-MRI and HF-MRI, the results may be confounded by the different DBM configurations. Moreover, as described in the Segmentation of baseline images section, the definitions of the HF anatomical ROI in the labeling protocols for T1-MRI and HF-MRI have some differences. This can lead to an additional confound due to the local volume change being integrated over different anatomical extents. On the other hand, if the definitions are kept the same, i.e., by propagating an HF ROI drawn in one modality into the other modality, confounds due to misregistration between modalities may be present. To test whether these confounds affect our measurements, we carry out additional experiments that measure hippocampal atrophy rate in HF-MRI and T1-MRI using different combinations of linear registration approach (WB-RIGID or ROI-RIGID), domain of deformable registration (3D or 2D) and the modality where HF is labeled.

Subfield atrophy rate estimates from HF-MRI

We measure longitudinal atrophy rates from HF-MRI within 10 ROIs. These were: the whole hippocampus, 3 ROIs that coarsely subdivide the whole hippocampus (HEAD, BODY and TAIL), 3 ROIs that are labeled within the BODY (CA1, CA4DG and CA234DG), and 3 ROIs other than the hippocampus proper (SUB, ERC, PHG). Measured change within subfields in pseudo-longitudinal experiments from test–retest data is also reported.

Results

Feasibility of HF-MRI for longitudinal measurements: comparison with T1-MRI

In this section, we compare the atrophy rates in the whole hippocampus measured in HF-MRI (using methods described in the Processing pipeline for longitudinal change measurements from HF-MRI section; ROI-RIGID, 2D) and in T1-MRI (using methods described in the Processing pipeline for longitudinal change measurements from T1-MRI section; WB-RIGID, 3D). Atrophy rates for all subjects are plotted in the scatter diagram of Fig. 4. T1-MRI and HF-MRI measurements are plotted against each other on the x- and y-axis, respectively. The primary observation is that longitudinal measurements derived from the two modalities are generally consistent and significantly correlated with each other, and there are only a few subjects with substantially different atrophy rate estimates. Also, T1-MRI measurements appear to be slightly higher than the corresponding HF-MRI measurements ($p=0.05$, one-sided paired t-test).

Bar graphs in Fig. 4 summarize the mean atrophy rate data in the scatter plots in both patient and control groups. Significant non-zero longitudinal change was measured in both modalities in the patient group, but only in T1-MRI in controls. Significant cross-sectional effects of greater atrophy rates in patients than in controls were found in both experiments. However, this effect was stronger with HF-MRI measurements. This is indicated by the larger effect size (Δ), as well as lower estimated sample sizes (N). T-statistical maps of the cross-sectional effect in both modalities are shown in Fig. 5, visualized in a common atlas space. One can see the greater spatial variation in group effects in HF-MRI (panel (b)) compared to T1-MRI (panel (a)), indicating the suitability of HF-MRI for subregional

analysis that we present in the Longitudinal atrophy rates within hippocampal subfields section below.

Test–retest experiments

Figs. 6(a),(b) compare the measured *whole hippocampal change* between repeat scans using T1-MRI and HF-MRI. Measurements from both modalities were free of statistically significant additive bias (p=0.36 T1-MRI, p=0.17 HF-MRI). The absolute value of the change measurement provides an estimate of test–retest error. HF-MRI had a lower test–retest error than T1-MRI in 7 of 9 subjects, although a pairwise comparison did not reach statistical significance (one-sided paired *t*-test p=0.06). Fig. 6(c) plots the difference in orientation between oblique coronal slabs in the repeat HF-MRI scans against the measured change. The two quantities were not significantly correlated in our dataset (r=−0.49, p=0.18). However, we should interpret these results with caution because of the small size of our test–retest dataset, as this can still affect the measurements in an unpredictable manner.

Effect of DBM configurations and labeling confounds on atrophy rate measurements

In the previous two sections, we presented hippocampal atrophy rates obtained in a clinical cohort and a test–retest cohort using DBM in T1- and HF-MRI. We found that HF-MRI measurements were at least as sensitive as T1-MRI, free of additive bias, had lower test–retest error, and exhibited slightly stronger group effects. In this section, we summarize experiments using different combinations of DBM configurations and ROIs labeled in both modalities in Table 1. This will help evaluate, to what extent, these results reflect the inherent differences between information present in the modalities.

The primary observation from Table 1 is that alternative DBM configurations did not improve effect sizes obtained in either modality compared to the results presented in the Feasibility of HF-MRI for longitudinal measurements: comparison with T1-MRI section (rows 1 and 8). Neither did the effect size improve from changing the anatomical definition of the HF used for measuring atrophy rate (rows 2 and 4). The conventional approach using WB-RIGID and 3D registration, with the HF segmentation derived in T1-MRI, yielded the strongest effect size in T1-MRI (row 1). Likewise, ROI-RIGID with 2D registration and HF definition derived from HF-MRI produced the strongest effect size in HF-MRI (row 8).

Note that not all 16 possible combinations of DBM modality, linear registration approach, dimensionality of deformable registration and modality of HF segmentation, were examined. For instance, we did not use 2D registration in T1-MRI, which has isotropic spatial resolution. Likewise, we did not use HF ROI defined in T1-MRI for DBM in HF-MRI, because the posterior extent of the HF label, when mapped to HF-MRI, often falls outside the field of view, as HF-MRI only partially images the hippocampal tail region. However, from comparing rows 5, 6 with rows 1, 3 respectively, it can be observed that even when 3D registration is used in both HF-MRI and T1-MRI, the effect size is stronger in HF-MRI. Likewise, rows 2 and 5 show that when segmentation derived from HF-MRI is used for both T1-MRI and HF-MRI atrophy rate measurements, HF-MRI yields a bigger effect size, although possible registration error when mapping HF segmentation to T1-MRI may partly explain the poorer effect size in T1-MRI. Overall, this demonstrates that the slightly stronger effect sizes for HF-MRI in the Feasibility of HF-MRI for longitudinal measurements: comparison with T1-MRI section appear to arise from the inherent properties of this modality, and are not a confound of the specific methodological choices or anatomical definitions used in the DBM pipelines.

Longitudinal atrophy rates within hippocampal subfields

Fig. 7 plots average atrophy rates measured in 10 ROIs using HF-MRI, in both the clinical and test–retest cohorts. The pseudo atrophy rates for the test–retest experiments are plotted with green bars; as expected, none of the ROIs, including whole hippocampus, showed any significant non-zero measurement indicating the absence of additive bias in the measurements. No ROI had significant non-zero atrophy rate in controls. Significant positive atrophy rate was found in patients in most ROIs within the hippocampus proper. All three coarse subdivisions along the long axis had significant atrophy in patients, with the TAIL region showing the largest cross-sectional effect of greater atrophy rate in patients with the smallest estimated sample size. Within the BODY, CA4DG had the highest average atrophy rate, and CA1 showed the largest cross-sectional effect. The three ROIs outside of hippocampus proper – SUB, ERC and PHG – had high variability and no significant group effects. Even though no subfield within the BODY had greater statistical power in separating patients and controls than the whole hippocampus, we note that HEAD and TAIL subregions showed relatively large effect sizes, with TAIL having an effect size greater than the whole hippocampus. We observe in Fig. 5(b) that the posterior hippocampus (TAIL) region had a strong effect.

Discussion

Evaluating HF-MRI for longitudinal measurements

We used an indirect validation approach for longitudinal measurements using HF-MRI, where atrophy rates obtained using two modalities in the same subjects were compared with each other. Direct gold standard measurements are not available for longitudinal analysis, as opposed to volumetry where manual labeling is usually considered the gold standard. Atrophy rates measured by independent manual labeling of ROIs to measure volume changes in serial images tend to have large variances (Fox et al., 2005; Kaye et al., 2005; Jack et al., 2003), sometimes even an order of magnitude larger than the expected range of atrophy rates being measured (Schuff et al., 2009). Some researchers have used simulation studies where a known deformation field is applied to the baseline image, and is subsequently recovered by the method under evaluation (Camara et al., 2006; Camara et al., 2008; Karaçali and Davatzikos, 2006). These approaches may not always produce deformations that are anatomically plausible, and it is difficult to know if they faithfully mimic the tissue shrinkage and the image acquisition process. Also, the simulated deformations are often drawn from a statistical distribution with a certain kind of spatial regularization, which may be similar to the regularization model of the deformable transformation that is used to recover the induced deformation, making the measurements biased. Thus, we resort to the comparison with T1-MRI, as well as looking at the strength of expected group effects in a clinical cohort. We think it is a reasonable approach to take, considering that longitudinal measurements using T1-MRI represent the state-of-the-art, and will help begin to judge the utility of HF-MRI for making longitudinal measurements. One limitation of this approach lies in the unavailability of validation data on subfield-specific atrophy rates using DBM.

Data presented in Fig. 4 demonstrate that longitudinal measurements in the whole hippocampus using HF-MRI is at least as sensitive as those using T1-MRI. Given that HF-MRI has better intensity contrast in the hippocampal region, and a much higher in-plane resolution, it is conceivable that HF-MRI provides a more sensitive measurement of local change. We hypothesized that ROI-RIGID global registration and 2D deformable registration will be appropriate for longitudinal analysis in HF-MRI, and it showed the strongest effect size. Independent alignment of hemispheres with ROI-RIGID and independent alignment of slices with 2D registration may have produced more accurate

alignments because of anisotropy. Fig. 3 shows the difference images after global and deformable registration. Better rigid alignment with ROI-RIGID in panel (d), compared to panel (c), may result in better deformable alignment, as shown by the arrows in panels (e) and (f).

Despite these differences described above, results in Table 1 showed the sensitivity of HF-MRI does not arise due to this specific DBM configuration used, but rather is a result of the inherent properties of the modality. Therefore, although our data do not prove that the specific combination of ROI-RIGID and 2D approach per se will always produce more sensitive measurements, it does show that HF-MRI is a viable modality for longitudinal analysis of the HF. Also, using effect size as the yardstick for evaluating different approaches, although practical, does not directly measure accuracy. Further evaluation is required, either using alternative evaluation criterion, or in a more well-characterized larger dataset where a strong clinical hypotheses would lend more confidence in the use of effect size. We also recognize that there are many parameters of the DBM pipeline that can affect measurements that we have not analyzed here. These include the type of similarity metric, the amount and nature of regularization in the deformable mapping, the transformation model chosen, the multi-resolution parameters and the step size parameter in ANTs. However, many of these are general aspects of DBM that may require optimization in any application that uses such methods.

The T1-MRI atrophy rate estimates were slightly higher on average than those using HF-MRI. One explanation for this is that if a substantial portion of the ROI undergoes volume reduction, the regularization of the deformation field can mask regions that do not — resulting in a higher atrophy rate estimate. As the deformable registration used a smoothness parameter that is scaled with the voxel size of the respective modalities (see ANTs parameters in the Deformable registration section), the effect of regularization spans a larger region in T1-MRI, owing to its larger voxel-size. One indication of this effect can be seen in the t-maps of Fig. 5, where HF-MRI has a more spatially varying pattern of effects than T1-MRI.

Bias in longitudinal measurements and sources of error

Sources of possible bias have been characterized and discussed by several authors (Fox et al., 2011; Hua et al., 2011; Reuter et al., 2010; Thompson et al., 2011; Yushkevich et al., 2010a). Results in the test–retest cohorts (Figs. 6 and 7) indicate that measurements in the whole hippocampus as well as in the subfields from HF-MRI are free of additive bias, as no significant non-zero change was expected between MRI scans acquired on the same day. However, other sources of numerical bias, e.g. a multiplicative bias, cannot be ruled out. Further, as we did not have a strong a priori hypothesis of expected patterns of atrophy across subfields, we cannot rule out the possibility that the observed variations of atrophy rates across subfields are partly a result of some methodological artifact that imposes a systematic pattern of *spatial bias* in our measurements.

Measurement error had a trend of negative correlation (Fig. 6, $r=-0.49$) with the difference in slice angle orientations between serial scans, although it was not significant ($p=0.18$). This is a potential source of confound in longitudinal measurements. We have now implemented a technique to automate the slice prescription of the followup HF-MRI scan to match that of the baseline scan. After the followup T1-MRI is acquired, it is registered with the baseline T1-MRI, and this information is utilized to generate the desired slab positioning parameters and used by the operator for planning the subsequent acquisition of HF-MRI so that its relative orientation to T1-MRI is similar to that of the baseline scan. This technique will be used in future longitudinal studies. There are other sources of variability that may be

beyond the experimenter's control, such as differences in ambient temperature, magnetic field uniformity and other scanner-related artifacts that may affect image appearance.

Subfield atrophy rate estimates from HF-MRI

A major appeal of HF-MRI has been the ability to make measurements at the level of subfields. As boundaries between the hippocampal subfields, particularly those between the CA and DG subregions, are better visible in HF-MRI — subfield-level volumetry has been possible (Mueller et al., 2009; Mueller et al., 2010) using subfield ROIs labeled in this modality. Could longitudinal change also be measured within these small subregions? Unlike measurements made within the whole hippocampus, there was no a priori specific hypothesis about the nature and magnitude of expected atrophy rates within specific subfields. Sometimes prior hypotheses about the expected group effects may be available from the clinical nature of the dataset. Even though our patient cohort included 7 individuals diagnosed with amnesic MCI, the remaining 8 were only classified as cognitively impaired, non-demented. In some of the subjects, the diagnostic classification had changed over time. In these instances, we used the diagnosis at their latest clinic visit. This made the cohort heterogeneous, and contributed to the lack of information for clinical validation of our measurements. This could also explain why the average atrophy rates in the whole hippocampus in patients are lower in our dataset (<1.5% in patients) than what other studies have reported in MCI (e.g., in (Schuff et al., 2009)). Under these constraints, the results of subfield atrophy rate measurements have to be interpreted with caution.

In controls, we did not find any significant atrophy in any ROI (Fig. 7). The largest mean atrophy rate in patients was seen in the TAIL, and in CA4DG in the BODY region, although CA4DG and CA234DG measurements also had the largest variance. Significant group difference in atrophy rates was found between patients and controls in all ROIs in the body (CA1, CA4DG and CA234DG), and in TAIL. While atrophy in CA1 is expected in aMCI, which is a preclinical stage of Alzheimer's disease in which CA1 pathology has been well-described (Jacobsen et al., 2006) and volumetric effects have been found (Mueller et al., 2010), atrophy in CA4DG/CA234DG has not been validated in pathology. However, as discussed above, our patient cohort is heterogenous and only about half of them are diagnosed as aMCI — thus it is unclear what kind of spatial atrophy pattern is expected inside the hippocampus. Nonetheless, we note that presence of atrophy in MCI in CA4DG and CA3 has been recently reported in a cross-sectional structural morphometry study (Yassa et al., 2010). The effects in the other two coarse subregions of the hippocampus proper – HEAD and TAIL – both of which contain CA and DG subfields, may be due to specific change within one or more of these subfields. However, this can only be studied with a subfield label that spans the entire length of the hippocampus. In the current protocol, it is difficult to label CA/DG subfields consistently in the HEAD and TAIL regions. Availability of histological data can enable complete subfield labeling, and is part of our ongoing work. The strong effect in TAIL may in part be an artifact of the TAIL being only partially imaged in HF-MRI, particularly if there is non-uniform atrophy along the length of ROI. For instance, if the anterior (imaged) portions of the TAIL have a disproportionately greater atrophy in patients than the non-imaged posterior region, this may result in stronger-than-expected group effects when measured over the partially imaged ROI. MRI sequences capable of collecting more slices may help resolve this confound in future studies.

As such, the subfield atrophy rate measurements reported here – the first time such measurements have been attempted in HF-MRI – should be considered preliminary. However, the results are promising, especially with whole hippocampus measurements — indicating that HF-MRI may be useful for longitudinal measurements in clinical trials.

Alternative measures of longitudinal change

DBM is a widely used technique in measuring longitudinal change in clinical populations, but a number of other measures of change have been used. DBM falls under the class of methods that attempts to measure local volume change. Manual, independent labeling of longitudinal images (Schuff et al., 2009) also measures volume change, directly over an ROI. There are 4D automatic segmentation techniques that simultaneously label ROIs in serial images (Wolz et al., 2010). Brain boundary shift integral (BSI) (Freeborough and Fox, 1997) and its derivative techniques (Leung et al., 2010) attempt to measure change directly within the region based on intensity patterns. Another useful metric is cortical thickness which has been thought to complement volumetric measurements (Burggren et al., 2008), although most methodologies that generate a whole brain cortical thickness map are less reliable in the MTL than in regions of neocortex (Wonderlick et al., 2009). Longitudinal measurements of thickness change also have some limitations due to its dependence on consistency of cortical gray matter segmentation (Nakamura et al., 2011). Nonetheless, it has been successfully used to study longitudinal change in clinical studies (Das et al., 2009; Li et al., 2011). Relevant to the current study, Donix et al. (2010) reported significant group effects of longitudinal changes in thickness in hippocampal subfields using a cortical flattening technique that was independently applied to baseline and followup HF-MRI data. This study used independent manual labeling of the longitudinal image pair, and did not directly compare the images, unlike most automated longitudinal analyses techniques, including ours.

Conclusion

The main goal of this paper was an evaluation of high-resolution in vivo T2-MRI for measuring longitudinal atrophy rate in the hippocampal formation using an unbiased deformation-based morphometry pipeline, with minor modifications to address characteristics of this modality. We approached this task by comparing whole hippocampal atrophy rate measurements using HF-MRI and the more commonly acquired T1-MRI, in a longitudinal dataset that includes serial images in both modalities for the same subjects. We found HF-MRI to be slightly more sensitive in detecting group effects, and this was not a result of variations of DBM methodology used with HF-MRI. Measurements were also shown to be free of additive bias. We also presented a preliminary study of hippocampal subfield atrophy rate estimates from HF-MRI.

In conclusion, this work showed that HF-MRI is a viable modality for making longitudinal measurements in the hippocampal formation. However, further evaluation necessary, especially for subfield-specific measurements, particularly in light of the future availability of such data in large multi-site studies such as ADNI2 (Weiner et al., 2010).

Acknowledgments

This work was supported by the Penn-Pfizer Alliance grant 10295 (PY) and the NIH grants K25 AG027785 (PY), 1R01 AG037376-01 (PY), R21 NS061111 (PY), 2U01 AG024904-06 (MW), 1RC2 AG036535-01 (MW) and R01 AG010897 (MW).

References

Amaral DG, Lavenex P. Hippocampal neuroanatomy. The Hippocampus Book. 2007:37–129.

Apostolova LG, Mosconi L, Thompson PM, Green AE, Hwang KS, Ramirez A, Mistur R, Tsui WH, de Leon MJ. Subregional hippocampal atrophy predicts Alzheimer's dementia in the cognitively normal. Neurobiol. Aging. 2010; 31(7):1077–1088. 7. [PubMed: 18814937]

Avants BB, Epstein CL, Grossman M, Gee JC. Symmetric diffeomorphic image registration with cross-correlation: evaluating automated labeling of elderly and neurodegenerative brain. Med. Image Anal. 2008; 12(1):26–41. 2. [PubMed: 17659998]

Barnes J, Scahill RI, Boyes RG, Frost C, Lewis EB, Rossor CL, Rossor MN, Fox NC. Differentiating AD from aging using semiautomated measurement of hippocampal atrophy rates. NeuroImage. 2004; 23(2):574–581. [PubMed: 15488407]

Barnes J, Bartlett JW, van de Pol LA, Loy CT, Scahill RI, Frost C, Thompson P, Fox NC. A meta-analysis of hippocampal atrophy rates in Alzheimer's disease. Neurobiol. Aging. 2009; 30(11): 1711–1723. 11. [PubMed: 18346820]

Beckett LA, Harvey DJ, Gamst A, Donohue M, Kornak J, Zhang H, Kuo JH, Initiative ADN. The Alzheimer's disease neuroimaging initiative: annual change in biomarkers and clinical outcomes. Alzheimers Dement. 2010; 6(3):257–264. 5. [PubMed: 20451874]

Bobinski M, Wegiel J, Tarnawski M, Reisberg B, de Leon MJ, Miller DC, Wisniewski HM. Relationships between regional neuronal loss and neurofibrillary changes in the hippocampal formation and duration and severity of Alzheimer disease. J. Neuropathol. Exp. Neurol. 1997; 56(4):414–420. 4. [PubMed: 9100672]

Bogerts B, Lieberman JA, Ashtari M, Bilder RM, Degreef G, Lerner G, Johns C, Masiar S. Hippocampus–amygdala volumes and psychopathology in chronic schizophrenia. Biol. Psychiatry. 1993; 33(4):236–246. 2. [PubMed: 8471676]

Braak H, Braak E. Neuropathological stageing of Alzheimer-related changes. Acta Neuropathol. 1991; 82(4):239–259. [PubMed: 1759558]

Burggren AC, Zeineh MM, Ekstrom AD, Braskie MN, Thompson PM, Small GW, Bookheimer SY. Reduced cortical thickness in hippocampal subregions among cognitively normal apolipoprotein E e4 carriers. NeuroImage. 2008; 41(4):1177–1183. 7. [PubMed: 18486492]

Camara O, Schweiger M, Scahill RI, Crum WR, Sneller BI, Schnabel JA, Ridgway GR, Cash DM, Hill DLG, Fox NC. Phenomenological model of diffuse global and regional atrophy using finite-element methods. IEEE Trans. Med. Imaging. 2006; 25(11):1417–1430. 11. [PubMed: 17117771]

Camara O, Schnabel JA, Ridgway GR, Crum WR, Douiri A, Scahill RI, Hill DLG, Fox NC. Accuracy assessment of global and local atrophy measurement techniques with realistic simulated longitudinal Alzheimer's disease images. NeuroImage. 2008; 42(2):696–709. 8. [PubMed: 18571436]

Caroli A, Frisoni GB, Initiative ADN. The dynamics of Alzheimer's disease biomarkers in the Alzheimer's Disease Neuroimaging Initiative cohort. Neurobiol. Aging. 2010; 31(8):1263–1274. 8. [PubMed: 20538373]

Chan D, Fox NC, Scahill RI, Crum WR, Whitwell JL, Leschziner G, Rossor AM, Stevens JM, Cipolotti L, Rossor MN. Patterns of temporal lobe atrophy in semantic dementia and Alzheimer's disease. Ann. Neurol. 2001; 49(4):433–442. 4. [PubMed: 11310620]

Chung MK, Worsley KJ, Paus T, Cherif C, Collins DL, Giedd JN, Rapoport JL, Evans AC. A unified statistical approach to deformation-based morphometry. NeuroImage. 2001; 14(3):595–606. 9. [PubMed: 11506533]

Csernansky JG, Wang L, Joshi S, Miller JP, Gado M, Kido D, McKeel D, Morris JC, Miller MI. Early DAT is distinguished from aging by high-dimensional mapping of the hippocampus. Dementia of the Alzheimer type. Neurology. 2000; 55(11):1636–1643. 12. [PubMed: 11113216]

Das SR, Avants BB, Grossman M, Gee JC. Registration based cortical thickness measurement. NeuroImage. 2009; 45(3):867–879. 4. [PubMed: 19150502]

de Leon MJ, Convit A, DeSanti S, Bobinski M, George AE, Wisniewski HM, Rusinek H, Carroll R, Saint Louis LA. Contribution of structural neuroimaging to the early diagnosis of Alzheimer's disease. Int. Psychogeriatr. 1997; 9(Suppl 1):183–190. discussion 247–52. [PubMed: 9546819]

De Vita E, Thomas DL, Roberts S, Parkes HG, Turner R, Kinchesh P, Shmueli K, Yousry TA, Ordidge RJ. High resolution MRI of the brain at 4.7 Tesla using fast spin echo imaging. Br. J. Radiol. 2003; 76(909):631–637. 9. [PubMed: 14500278]

Donix M, Burggren AC, Suthana NA, Siddarth P, Ekstrom AD, Krupa AK, Jones M, Rao A, Martin-Harris L, Ercoli LM, Miller KJ, Small GW, Bookheimer SY. Longitudinal changes in medial

temporal cortical thickness in normal subjects with the APOE-4 polymorphism. NeuroImage. 2010; 53(1):37–43. 10. [PubMed: 20541611]

Du AT, Schuff N, Kramer JH, Ganzer S, Zhu XP, Jagust WJ, Miller BL, Reed BR, Mungas D, Yaffe K, Chui HC, Weiner MW. Higher atrophy rate of entorhinal cortex than hippocampus in AD. Neurology. 2004; 62(3):422–427. 2. [PubMed: 14872024]

Duvernoy, H. Functional anatomy, vascularization, and serial sections with MRI. 3rd edition. Springer-Verlag; Berlin, New York: 2005. The human hippocampus.

Eriksson SH, Thom M, Bartlett PA, Symms MR, McEvoy AW, Sisodiya SM, Duncan JS. Propeller MRI visualizes detailed pathology of hippocampal sclerosis. Epilepsia. 2008; 49(1):33–39. 1. [PubMed: 17877734]

Fox NC, Warrington EK, Stevens JM, Rossor MN. Atrophy of the hippocampal formation in early familial Alzheimer's disease. A longitudinal MRI study of at-risk members of a family with an amyloid precursor protein 717Val-Gly mutation. Ann. N. Y. Acad. Sci. 1996; 777:226–232. 1. [PubMed: 8624089]

Fox NC, Cousens S, Scahill R, Harvey RJ, Rossor MN. Using serial registered brain magnetic resonance imaging to measure disease progression in Alzheimer disease: power calculations and estimates of sample size to detect treatment effects. Arch. Neurol. 2000; 57(3):339–344. 3. [PubMed: 10714659]

Fox NC, Black RS, Gilman S, Rossor MN, Griffith SG, Jenkins L, Koller M, AN1792(QS-21)-201 Study. Effects of Abeta immunization (AN1792) on MRI measures of cerebral volume in Alzheimer disease. Neurology. 2005; 64(9):1563–1572. 5. [PubMed: 15883317]

Fox NC, Ridgway GR, Schott JM. Algorithms, atrophy and Alzheimer's disease: cautionary tales for clinical trials. NeuroImage. 2011; 57(1):15–18. [PubMed: 21296168]

Freeborough PA, Fox NC. The boundary shift integral: an accurate and robust measure of cerebral volume changes from registered repeat MRI. IEEE Trans. Med. Imaging. 1997; 16(5):623–629. 10. [PubMed: 9368118]

Fuerst D, Shah J, Shah A, Watson C. Hippocampal sclerosis is a progressive disorder: a longitudinal volumetric MRI study. Ann. Neurol. 2003; 53(3):413–416. 3. [PubMed: 12601713]

Geuze E, Vermetten E, Bremner JD. MR-based in vivo hippocampal volumetrics: 2. Findings in neuropsychiatric disorders. Mol. Psychiatry. 2005; 10(2):160–184. 2. [PubMed: 15356639]

Hashimoto M, Kazui H, Matsumoto K, Nakano Y, Yasuda M, Mori E. Does donepezil treatment slow the progression of hippocampal atrophy in patients with Alzheimer's disease? Am. J. Psychiatry. 2005; 162(4):676–682. 4. [PubMed: 15800138]

Holland D, McEvoy LK, Dale AM, the Alzheimer's Disease Neuroimaging Initiative. Unbiased comparison of sample size estimates from longitudinal structural measures in adni. Hum. Brain Mapp. 2011:8.

Hua X, Gutman B, Boyle CP, Rajagopalan P, Leow AD, Yanovsky I, Kumar AR, Toga AW, Jack CR, Schuff N, Alexander GE, Chen K, Reiman EM, Weiner MW, Thompson PM, the Alzheimer's Disease Neuroimaging Initiative. Accurate measurement of brain changes in longitudinal MRI scans using tensor-based morphometry. NeuroImage. 2011; 57(1):5–14. 7. [PubMed: 21320612]

Huesgen CT, Burger PC, Crain BJ, Johnson GA. In vitro MR microscopy of the hippocampus in Alzheimer's disease. Neurology. 1993; 43(1):145–152. 1. [PubMed: 8423879]

Jack CR, Petersen RC, O'Brien PC, Tangalos EG. MR-based hippocampal volumetry in the diagnosis of Alzheimer's disease. Neurology. 1992; 42(1):183–188. 1. [PubMed: 1734300]

Jack CR, Petersen RC, Xu Y, O'Brien PC, Smith GE, Ivnik RJ, Tangalos EG, Kokmen E. Rate of medial temporal lobe atrophy in typical aging and Alzheimer's disease. Neurology. 1998; 51(4): 993–999. 10. [PubMed: 9781519]

Jack CR, Petersen RC, Xu Y, O'Brien PC, Smith GE, Ivnik RJ, Boeve BF, Tangalos EG, Kokmen E. Rates of hippocampal atrophy correlate with change in clinical status in aging and AD. Neurology. 2000; 55(4):484–489. 8. [PubMed: 10953178]

Jack CR, Slomkowski M, Gracon S, Hoover TM, Felmlee JP, Stewart K, Xu Y, Shiung M, O'Brien PC, Cha R, Knopman D, Petersen RC. MRI as a biomarker of disease progression in a therapeutic trial of milameline for AD. Neurology. 2003; 60(2):253–260. 1. [PubMed: 12552040]

Jack CR, Bernstein MA, Borowski BJ, Gunter JL, Fox NC, Thompson PM, Schuff N, Krueger G, Killiany RJ, Decarli CS, Dale AM, Carmichael OW, Tosun D, Weiner MW, Alzheimer's Disease Neuroimaging Initiative. Update on the magnetic resonance imaging core of the Alzheimer's disease neuroimaging initiative. Alzheimers Dement. 2010; 6(3):212–220. 5. [PubMed: 20451869]

Jacobsen JS, Wu C-CC, Redwine JM, Comery TA, Arias R, Bowlby M, Martone R, Morrison JH, Pangalos MN, Reinhart PH, Bloom FE. Early-onset behavioral and synaptic deficits in a mouse model of Alzheimer's disease. Proc. Natl. Acad. Sci. U. S. A. 2006; 103(13):5161–5166. 3. [PubMed: 16549764]

Karaçali B, Davatzikos C. Simulation of tissue atrophy using a topology preserving transformation model. IEEE Trans. Med. Imaging. 2006; 25(5):649–652. 5. [PubMed: 16689268]

Kaye JA, Moore MM, Dame A, Quinn J, Camicioli R, Howieson D, Corbridge E, Care B, Nesbit G, Sexton G. Asynchronous regional brain volume losses in presymptomatic to moderate AD. J. Alzheimers Dis. 2005; 8(1):51–56. 9. [PubMed: 16155349]

Kerchner GA, Hess CP, Hammond-Rosenbluth KE, Xu D, Rabinovici GD, Kelley DAC, Vigneron DB, Nelson SJ, Miller BL. Hippocampal CA1 apical neuropil atrophy in mild Alzheimer disease visualized with 7-T MRI. Neurology. 2010; 75(15):1381–1387. 10. [PubMed: 20938031]

Kerwin WS, Osman NF, Prince JL. Bankman I. Image Processing and Analysis in Tagged Cardiac MRI. Handbook of Medical Imaging: Processing and Analysis. 2000

La Joie R, Fouquet M, Mézenge F, Landeau B, Villain N, Mevel K, Pélerin A, Eustache F, Desgranges B, Chételat G. Differential effect of age on hippocampal subfields assessed using a new high-resolution 3T MR sequence. NeuroImage. 2010:6.

Leow AD, Klunder AD, Jack CR, Toga AW, Dale AM, Bernstein MA, Britson PJ, Gunter JL, Ward CP, Whitwell JL, Borowski BJ, Fleisher AS, Fox NC, Harvey D, Kornak J, Schuff N, Studholme C, Alexander GE, Weiner MW, Thompson PM, ADNI Preparatory Phase Study. Longitudinal stability of MRI for mapping brain change using tensor-based morphometry. NeuroImage. 2006; 31(2):627–640. 6. [PubMed: 16480900]

Leung KK, Barnes J, Ridgway GR, Bartlett JW, Clarkson MJ, Macdonald K, Schuff N, Fox NC, Ourselin S, Alzheimer's Disease Neuroimaging Initiative. Automated cross-sectional and longitudinal hippocampal volume measurement in mild cognitive impairment and Alzheimer's disease. NeuroImage. 2010; 51(4):1345–1359. 7. [PubMed: 20230901]

Li Y, Wang Y, Wu G, Shi F, Zhou L, Lin W, Shen D, Initiative TADN. Discriminant analysis of longitudinal cortical thickness changes in Alzheimer's disease using dynamic and network features. Neurobiol. Aging. 2011:1. [PubMed: 20961659]

Malykhin NV, Lebel RM, Coupland NJ, Wilman AH, Carter R. In vivo quantification of hippocampal subfields using 4.7 T fast spin echo imaging. NeuroImage. 2010; 49(2):1224–1230. 1. [PubMed: 19786104]

Mueller SG, Stables L, Du AT, Schuff N, Truran D, Cashdollar N, Weiner MW. Measurement of hippocampal subfields and age-related changes with high resolution MRI at 4T. Neurobiol. Aging. 2007; 28(5):719–726. 5. [PubMed: 16713659]

Mueller SG, Schuff N, Raptentsetsang S, Elman J, Weiner MW. Selective effect of Apo e4 on CA3 and dentate in normal aging and Alzheimer's disease using high resolution MRI at 4 T. NeuroImage. 2008; 42(1):42–48. 8. [PubMed: 18534867]

Mueller SG, Laxer KD, Barakos J, Cheong I, Garcia P, Weiner MW. Subfield atrophy pattern in temporal lobe epilepsy with and without mesial sclerosis detected by high-resolution MRI at 4 Tesla: preliminary results. Epilepsia. 2009; 50(6):1474–1483. 6. [PubMed: 19400880]

Mueller SG, Schuff N, Yaffe K, Madison C, Miller B, Weiner MW. Hippocampal atrophy patterns in mild cognitive impairment and Alzheimer's disease. Hum. Brain Mapp. 2010; 31(9):1339–1347. 9. [PubMed: 20839293]

Nakamura K, Fox R, Fisher E. CLADA: cortical longitudinal atrophy detection algorithm. NeuroImage. 2011; 54(1):278–289. 1. [PubMed: 20674750]

Petersen RC, Smith GE, Waring SC, Ivnik RJ, Tangalos EG, Kokmen E. Mild cognitive impairment: clinical characterization and outcome. Arch. Neurol. 1999; 56(3):303–308. [PubMed: 10190820]

Pluta J, Avants BB, Glynn S, Awate S, Gee JC, Detre JA. Appearance and incomplete label matching for diffeomorphic template based hippocampus segmentation. Hippocampus. 2009; 19(6):565–571. 6. [PubMed: 19437413]

Prudent V, Kumar A, Liu S, Wiggins G, Malaspina D, Gonen O. Human hippocampal subfields in young adults at 7.0 T: feasibility of imaging. Radiology. 2010; 254(3):900–906. 3. [PubMed: 20123900]

Reuter M, Rosas HD, Fischl B. Highly accurate inverse consistent registration: a robust approach. NeuroImage. 2010; 53(4):1181–1196. 12. [PubMed: 20637289]

Ridha BH, Barnes J, Bartlett JW, Godbolt A, Pepple T, Rossor MN, Fox NC. Tracking atrophy progression in familial Alzheimer's disease: a serial MRI study. Lancet Neurol. 2006; 5(10):828–834. 10. [PubMed: 16987729]

Risacher SL, Shen L, West JD, Kim S, McDonald BC, Beckett LA, Harvey DJ, Jack CR, Weiner MW, Saykin AJ, Alzheimer's Disease Neuroimaging Initiative (ADNI; Risacher SL, Shen L, West JD, Kim S, McDonald BC, Beckett LA, Harvey DJ, Jack CR, Weiner MW, Saykin AJ, ADNI. Longitudinal MRI atrophy biomarkers: relationship to conversion in the ADNI cohort. Neurobiol. Aging. 2010; 31(8):1401–1418. 8. [PubMed: 20620664]

Rohrer JD, McNaught E, Foster J, Clegg SL, Barnes J, Omar R, Warrington EK, Rossor MN, Warren JD, Fox NC. Tracking progression in frontotemporal lobar degeneration: serial MRI in semantic dementia. Neurology. 2008; 71(18):1445–1451. 10. [PubMed: 18955688]

Saravia FE, Beauquis J, Revsin Y, Homo-Delarche F, de Kloet ER, De Nicola AF. Hippocampal neuropathology of diabetes mellitus is relieved by estrogen treatment. Cell. Mol. Neurobiol. 2006; 26(4–6):943–957. [PubMed: 16807785]

Sass KJ, Lencz T, Westerveld M, Novelly RA, Spencer DD, Kim JH. The neural substrate of memory impairment demonstrated by the intracarotid amobarbital procedure. Arch. Neurol. 1991; 48(1): 48–52. 1. [PubMed: 1986726]

Schott JM, Bartlett JW, Barnes J, Leung KK, Ourselin S, Fox NC, Alzheimer's Disease Neuroimaging Initiative investigators. Reduced sample sizes for atrophy outcomes in Alzheimer's disease trials: baseline adjustment 8 Neurobiol. Aging. 2010; 31(8):1452–1462. 1462.e1–2.

Schuff N, Woerner N, Boreta L, Kornfield T, Shaw LM, Trojanowski JQ, Thompson PM, Jack CR, Weiner MW, the Alzheimer's Disease Neuroimaging Initiative. MRI of hippocampal volume loss in early Alzheimer's disease in relation to apoe genotype and biomarkers. Brain. 2009; 132(Pt 4): 1067–1077. 2. [PubMed: 19251758]

Shewchuk, JR. Triangle: engineering a 2D quality mesh generator and delaunay triangulator. In: Lin, MC.; Manocha, D., editors. Applied Computational Geometry: Towards Geometric Engineering. Vol. Vol. 1148. Springer-Verlag; 1996. p. 203-222.p. 5Lecture Notes in Computer Science

Small SA, Nava AS, Perera GM, Delapaz R, Stern Y. Evaluating the function of hippocampal subregions with high-resolution MRI in Alzheimer's disease and aging. Microsc. Res. Tech. 2000; 51(1):101–108. 10. [PubMed: 11002358]

Smith SM, Zhang Y, Jenkinson M, Chen J, Matthews PM, Federico A, De Stefano N. Accurate, robust, and automated longitudinal and cross-sectional brain change analysis. NeuroImage. 2002; 17(1):479–489. 9. [PubMed: 12482100]

Smith SM, Jenkinson M, Woolrich MW, Beckmann CF, Behrens TEJ, Johansen-Berg H, Bannister PR, De Luca M, Drobnjak I, Flitney DE, Niazy RK, Saunders J, Vickers J, Zhang Y, De Stefano N, Brady JM, Matthews PM. Advances in functional and structural MR image analysis and implementation as FSL. NeuroImage. 2004; 23(Suppl 1):S208–S219. [PubMed: 15501092]

Squire LR, Stark CEL, Clark RE. The medial temporal lobe. Annu. Rev. Neurosci. 2004; 27:279–306. [PubMed: 15217334]

Steffens DC, McQuoid DR, Payne ME, Potter GG. Change in hippocampal volume on magnetic resonance imaging and cognitive decline among older depressed and nondepressed subjects in the neurocognitive outcomes of depression in the elderly study. Am. J. Geriatr. Psychiatry. 2011; 19(1):4–12. 1. [PubMed: 20808107]

Studholme C, Cardenas V, Blumenfeld R, Schuff N, Rosen HJ, Miller B, Weiner M. Deformation tensor morphometry of semantic dementia with quantitative validation. NeuroImage. 2004; 21(4): 1387–1398. 4. [PubMed: 15050564]

Theysohn JM, Kraff O, Maderwald S, Schlamann MU, de Greiff A, Forsting M, Ladd SC, Ladd ME, Gizewski ER. The human hippocampus at 7 T—in vivo MRI. Hippocampus. 2009; 19(1):1–7. 1. [PubMed: 18727048]

Thomas DL, De Vita E, Roberts S, Turner R, Yousry TA, Ordidge RJ. High-resolution fast spin echo imaging of the human brain at 4.7 T: implementation and sequence characteristics. Magn. Reson. Med. 2004; 51(6):1254–1264. 6. [PubMed: 15170847]

Thomas BP, Welch EB, Niederhauser BD, Whetsell WO, Anderson AW, Gore JC, Avison MJ, Creasy JL. High-resolution 7 T MRI of the human hippocampus in vivo. J. Magn. Reson. Imaging. 2008; 28(5):1266–1272. 11. [PubMed: 18972336]

Thompson PM, Toga AW. Anatomically driven strategies for high-dimensional brain image warping and pathology detection. Brain Warping. 1998:311–336.

Thompson PM, Schwartz C, Lin RT, Khan AA, Toga AW. Three-dimensional statistical analysis of sulcal variability in the human brain. J. Neurosci. 1996; 16(13):4261–4274. 7. [PubMed: 8753887]

Thompson PM, Hayashi KM, De Zubicaray GI, Janke AL, Rose SE, Semple J, Hong MS, Herman DH, Gravano D, Doddrell DM, Toga AW. Mapping hippocampal and ventricular change in Alzheimer disease. NeuroImage. 2004; 22(4):1754–1766. 8. [PubMed: 15275931]

Thompson WK, Holland D, the Alzheimer's Disease Neuroimaging Initiative. Bias in tensor based morphometry Stat-ROI measures may result in unrealistic power estimates. NeuroImage. 2011; 57(1):1–4. 7. [PubMed: 21349340]

Van Leemput K, Bakkour A, Benner T, Wiggins G, Wald LL, Augustinack J, Dickerson BC, Golland P, Fischl B. Automated segmentation of hippocampal subfields from ultra-high resolution in vivo MRI. Hippocampus. 2009; 19(6):549–557. 6. [PubMed: 19405131]

Wang L, Swank JS, Glick IE, Gado MH, Miller MI, Morris JC, Csernansky JG. Changes in hippocampal volume and shape across time distinguish dementia of the Alzheimer type from healthy aging. NeuroImage. 2003; 20(2):667–682. 10. [PubMed: 14568443]

Wang H, Das SR, Suh JW, Altinay M, Pluta J, Craige C, Avants B, Yushkevich PA. A learning-based wrapper method to correct systematic errors in automatic image segmentation: consistently improved performance in hippocampus, cortex and brain segmentation. NeuroImage. 2011; 55(3): 968–985. 1. [PubMed: 21237273]

Weiner MW, Aisen PS, Jack CR, Jagust WJ, Trojanowski JQ, Shaw L, Saykin AJ, Morris JC, Cairns N, Beckett LA, Toga A, Green R, Walter S, Soares H, Snyder P, Siemers E, Potter W, Cole PE, Schmidt M, Alzheimer's Disease Neuroimaging Initiative. The Alzheimer's disease neuroimaging initiative: progress report and future plans e7 Alzheimers Dement. 2010; 6(3):202–211. 5.

Wolz R, Heckemann RA, Aljabar P, Hajnal JV, Hammers A, Lőtjőnen J, Rueckert D, Alzheimer's Disease Neuroimaging Initiative. Measurement of hippocampal atrophy using 4d graph-cut segmentation: application to ADNI. NeuroImage. 2010; 52(1):109–118. 8. [PubMed: 20382238]

Wonderlick JS, Ziegler DA, Hosseini-Varnamkhasti P, Locascio JJ, Bakkour A, van der Kouwe A, Triantafyllou C, Corkin S, Dickerson BC. Reliability of MRI-derived cortical and subcortical morphometric measures: effects of pulse sequence, voxel geometry, and parallel imaging. NeuroImage. 2009; 44(4):1324–1333. 2. [PubMed: 19038349]

Yassa MA, Stark SM, Bakker A, Albert MS, Gallagher M, Stark CEL. High-resolution structural and functional MRI of hippocampal CA3 and dentate gyrus in patients with amnestic Mild Cognitive Impairment. NeuroImage. 2010; 51(3):1242–1252. 7. [PubMed: 20338246]

Yushkevich PA, Avants BB, Das SR, Pluta J, Altinay M, Craige C, Alzheimer's Disease Neuroimaging Initiative. Bias in estimation of hippocampal atrophy using deformation-based morphometry arises from asymmetric global normalization: an illustration in ADNI 3 T MRI data. NeuroImage. 2010a; 50(2):434–445. 4. [PubMed: 20005963]

Yushkevich PA, Wang H, Pluta J, Das SR, Craige C, Avants BB, Weiner MW, Mueller S. Nearly automatic segmentation of hippocampal subfields in in vivo focal T2-weighted MRI. NeuroImage. 2010b; 53(4):1208–1224. 6. [PubMed: 20600984]

Zeineh MM, Engel SA, Thompson PM, Bookheimer SY. Dynamics of the hippocampus during encoding and retrieval of face-name pairs. Science. 2003; 299(5606):577–580. 1. [PubMed: 12543980]

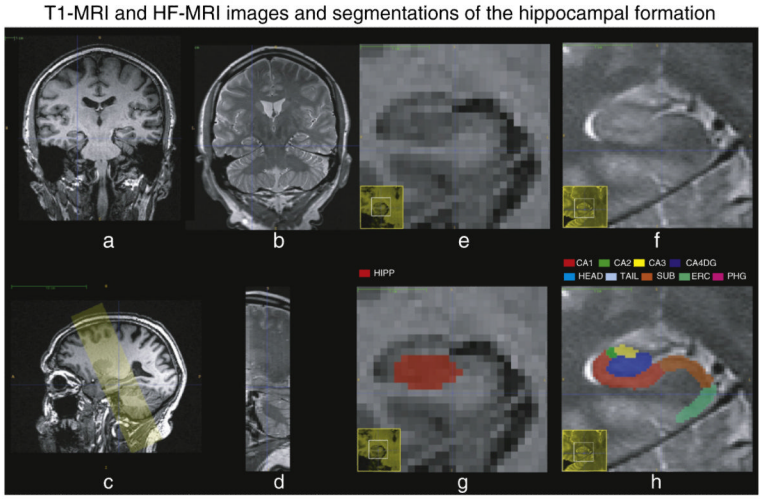

Fig. 1.

Example of T1-MRI and HF-MRI images for a subject. (a)–(d): Whole brain images. (a) Coronal view of T1-MRI, (b) oblique coronal slice from HF-MRI of the same subject as in (a) (0.4×0.4 mm resolution), (c) sagittal view of T1-MRI with the field of view of the obliquely oriented T2-weighted HF-MRI overlaid in light yellow, (d) sagittal cross-section of the HF-MRI, illustrating the anisotropy of the voxels. The voxel size is 2.0 mm along the anterior–posterior direction. (e)–(h) Enlarged view of the region around the right hippocampal formation in the coronal slice. (e) T1-MRI image, (f) HF-MRI image, (g) T1-MRI whole hippocampus label, (h) HF-MRI subfield labels. Insets in (e)–(h) show the extent of the ROI image used in the ROI-RIGID approach.

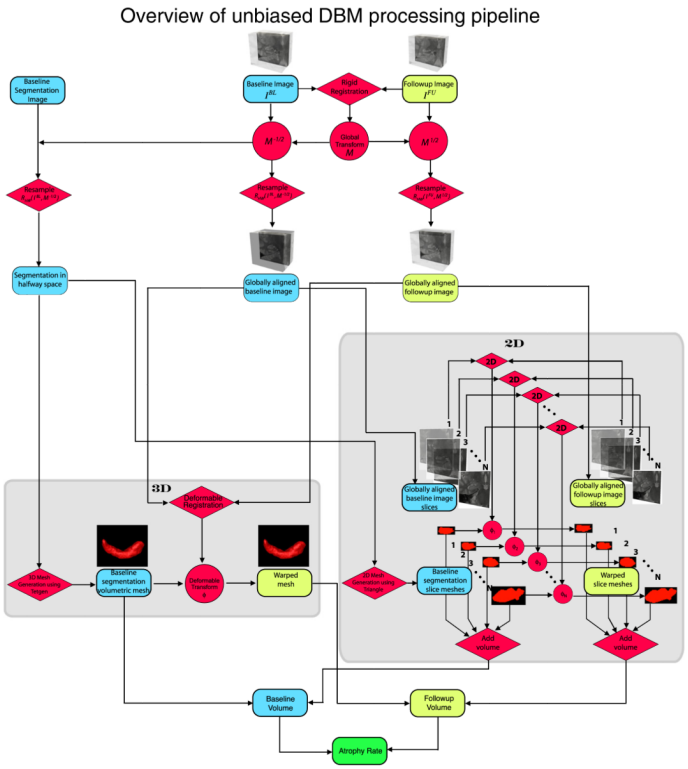

Fig. 2.

Flow diagram illustrating the processing steps in the unbiased DBM pipeline used in this study. Processing begins (top) with global registration of the serial image pair that consists of an ROI around the HF, which corresponds to the ROI-RIGID approach. Whole brain images can instead be used for the traditional WB-RIGID approach. The shaded area on the left shows processing used in 3D deformable mapping and is the same for T1- and HF-MRI. The shaded area on the right shows processing used in 2D deformable mapping, which is only used for HF-MRI. The baseline segmentation image is assumed to be already in the space of the DBM modality. The entire pipeline is repeated for left and right HF. See text for detailed description of each step.

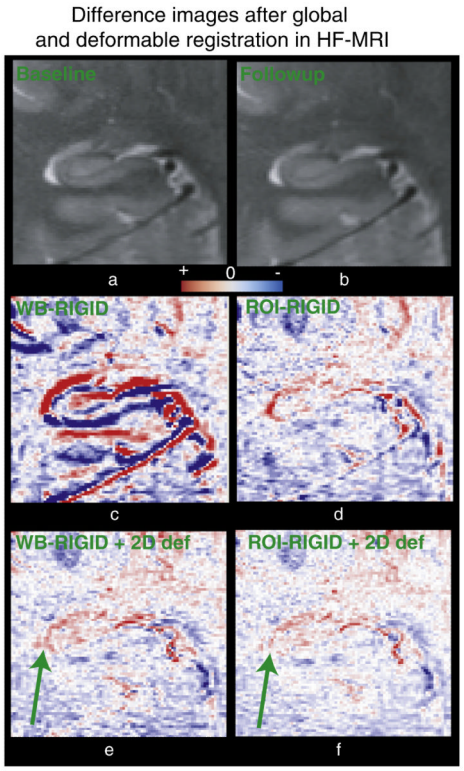

Fig. 3.

(a) Example of a baseline HF-MRI ROI image. (b) Followup HF-MRI of the same subject. (c) Difference image after linear registration using WB-RIGID. (d) Difference image after linear registration using ROI-RIGID. (e) Difference image after WB-RIGID and 2D deformable registration. (f) Difference image after ROI-RIGID and 2D deformable registration. White indicates zero difference and better alignment. All images are shown in the halfway space. Arrow indicates an area where ROI-RIGID, 2D provides better alignment than WB-RIGID, 2D.

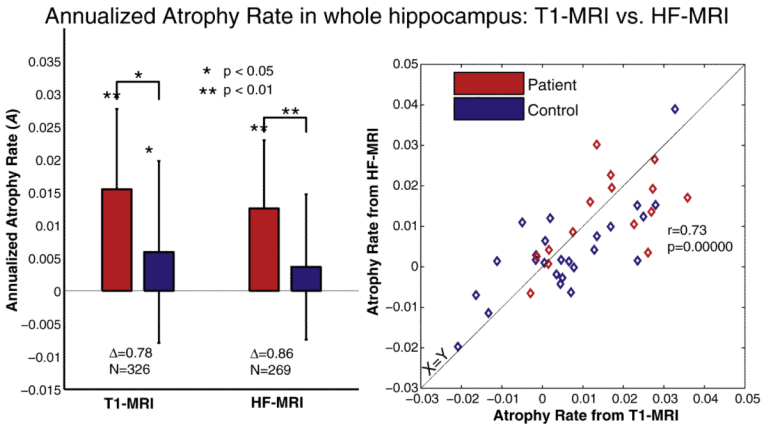

Fig. 4.

Comparison of annual atrophy rates derived using DBM in T1- and HF-MRI in patients and controls. Atrophy rate is computed from the whole hippocampus ROI and averaged over left and right sides. A value of 0.01 indicates 1% annualized loss in hippocampal volume. Error bars represent standard deviation. In the bar graphs on the left,"*"s on top of an error bar indicate significant non-zero atrophy rate measurement for the corresponding subject group, and those over the line connecting the bar graphs for two groups indicate significant cross-sectional difference in atrophy rates between the groups (patients>controls). In each case, effect size Δ and sample size estimate N (Eqs. (5) and (6)) are also shown. In the scatterplot on the right, each data point shows T1- and HF-MRI based atrophy rate estimates plotted against each other for one subject. Correlations between measurements from the two modalities are shown as well.

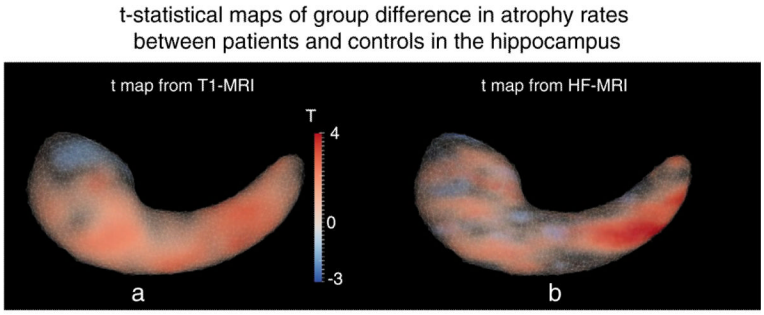

Fig. 5.

t-Statistical maps of significant group difference in atrophy rates between patients and controls as measured in T1-MRI (a) and HF-MRI (b), both from left hippocampi. Positive values indicate greater atrophy in patients. The t-maps were derived in the respective modalities and mapped to a common atlas space for the purpose of visualization.

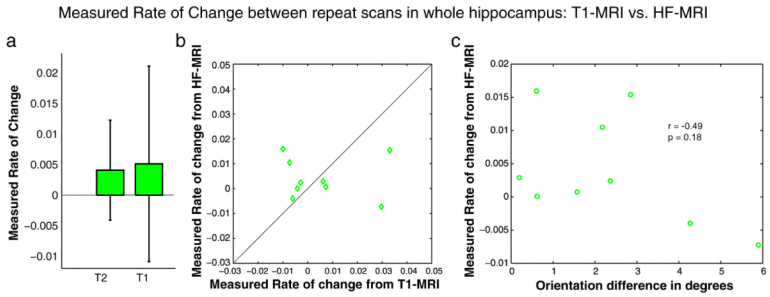

Fig. 6.

(a) and (b) show bar and scatter plots of putative measured *atrophy rate* from test–retest scan pairs in whole hippocampus using DBM in T1-MRI and HF-MRI. Error bars represent standard deviation. (c) Measured *atrophy rate* shown in (b) using DBM in HF-MRI is plotted against the angular difference in orientation of oblique coronal slices between baseline and followup scans. Correlation and p-value are shown.

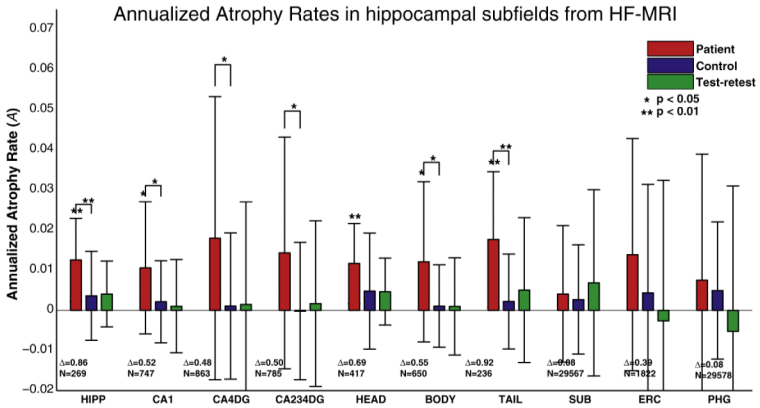

Fig. 7.

Estimated longitudinal atrophy rate from patients (red), controls (blue) and between repeat scans (green) from HF-MRI in hippocampal subfields. Atrophy rates are averaged over left and right sides. A value of 0.01 indicates 1% annualized loss in subfield volume. Error bars represent standard deviation. In the bar graphs on the left,"*"s on top of an error bar indicate significant non-zero atrophy rate measurement for the corresponding subject group, and those over the line connecting the bar graphs for two groups indicate significant cross-sectional difference in atrophy rates between the groups (patients > controls). In each case, effect size Δ and sample size estimate N (Eqs. (5) and (6)) are also shown.

Table 1

Estimates of annualized atrophy rate in whole hippocampus as defined in Eq. (4) using different DBM configurations. Configurations with the strongest effect sizes in both modalities are indicated in bold.

Expt. no.	DBM modality[a]	Labeling modality[b]	Global registration	Deformable registration	Control atrophy rate % $\mu(\sigma)$	Patient atrophy rate % $\mu(\sigma)$[c]	Effect size Δ	Sample size N
1	T1-MRI	T1-MRI	WB-RIGID	3D	0.59 (1.38)	1.55 (1.22) *	**0.78**	**325**
2	T1-MRI	HF-MRI	WB-RIGID	3D	0.40 (1.51)	1.20 (1.46) n.s.	0.56	661
3	T1-MRI	T1-MRI	ROI-RIGID	3D	0.55 (1.35)	1.50 (1.28) *	0.74	358
4	T1-MRI	HF-MRI	ROI-RIGID	3D	0.35 (1.50)	1.20 (1.42) *	0.60	556
5	HF-MRI	HF-MRI	WB-RIGID	3D	0.17 (0.93)	1.29 (1.37) **	0.82	298
6	HF-MRI	HF-MRI	ROI-RIGID	3D	0.17 (0.88)	1.18 (1.30) **	0.78	326
7	HF-MRI	HF-MRI	WB-RIGID	2D	0.36 (1.01)	1.18 (1.00) **	0.82	293
8	HF-MRI	HF-MRI	ROI-RIGID	2D	0.36 (1.11)	1.26 (1.04) **	**0.86**	**269**

[a] Modality where atrophy rate is measured with DBM.

[b] Modality where the segmentation of the HF is performed (slightly different anatomical definitions and longitudinal extents of the HF are used in HF-MRI and T1-MRI segmentation protocols).

[c] Result of one-sided two sample t-test (patient atrophy rate>control):

* $p<0.05$

** $p<0.01$, n.s.=not significant.